Plant Physiol. (1992) 99, 734–747
0032-0889/92/99/0734/14/$01.00/0

Received for publication October 3, 1991
Accepted January 24, 1992

Measurement of Net Fluxes of Ammonium and Nitrate at the Surface of Barley Roots Using Ion-Selective Microelectrodes[1]

II. Patterns of Uptake Along the Root Axis and Evaluation of the Microelectrode Flux Estimation Technique

Gordon H. Henriksen, D. Raj Raman, Larry P. Walker, and Roger M. Spanswick*

Section of Plant Biology, Division of Biological Sciences (G.H.H., R.M.S.), and Department of Agricultural and Biological Engineering (D.R.R., L.P.W.), Cornell University, Ithaca, New York 14853

ABSTRACT

Net fluxes of NH_4^+ and NO_3^- into roots of 7-day-old barley (*Hordeum vulgare* L. cv Prato) seedlings varied both with position along the root axis and with time. These variations were not consistent between replicate plants; different roots showed unique temporal and spatial patterns of uptake. Axial scans of NH_4^+ and NO_3^- net fluxes were conducted along the apical 7 centimeters of seminal roots of intact barley seedlings in solution culture using ion-selective microelectrodes in the unstirred layer immediately external to the root surface. Theoretically derived relationships between uptake and concentration gradients, combined with experimental observations of the conditions existing in our experimental system, permitted evaluation of the contribution of bulk water flow to ion movement in the unstirred layer, as well as a measure of the spatial resolution of the microelectrode flux estimation technique. Finally, a method was adopted to assess the accuracy of this technique.

Investigations of nutrient acquisition have relied primarily on techniques that integrate uptake over the entire root system. Unfortunately, this approach fails to reveal which regions of the root are actually involved in the uptake process. The localization of uptake along the root axis will assist in the correlation of root development, structure, metabolism, and transport processes. Because a progression of root cell maturation is observed as one moves basipetally from the apical meristem, it is reasonable to expect that cellular biochemistry and metabolic requirements may also vary with position along the root axis. In support of this expectation, it has been demonstrated that longitudinal gradients in respiratory activity (18) and nitrate assimilatory enzyme activity (21) occur along root axes of barley and maize, respectively. We, therefore, sought to discover whether the transport of inorganic nitrogen, as both NH_4^+ and NO_3^-, also exhibits a gradient along the root axis and follows these previously observed variations in metabolism.

Inorganic nitrogen occurs in the soil solution in two forms: the ammonium cation and the nitrate anion. The charge of the ion strongly influences whether transport will be thermodynamically favorable or require the expenditure of additional metabolic energy; it also determines which mechanism(s) might be used to maintain electroneutrality at the root-soil interface (12). Once transported into the cell, the energy cost of assimilation to glutamate differs between NH_4^+ and NO_3^-; the reduction of NO_3^- to NH_4^+ requires the equivalent of an additional 15 ATP (25). Furthermore, the assimilation of each ion affects cytoplasmic pH differently; the incorporation of NH_4^+ generates H^+, whereas the reduction of NO_3^- results in a net alkalinization of the cytosol. It has been suggested that, to maintain electroneutrality during transport and to regulate cytoplasmic pH during inorganic nitrogen assimilation, H^+ or OH^-/HCO_3^- ions are exported to the rhizosphere (12, 23). Indeed, it is generally observed that plants grown with NH_4^+ as the sole nitrogen source acidify the external medium. Conversely, when NO_3^- is the sole source of nitrogen, an alkalinization of the external medium occurs. In view of the differences between NH_4^+- and NO_3^--based nutrition, it seems likely that factors such as respiration and energy availability, enzyme activity, maintenance of electroneutrality, and plant nitrogen requirements would influence where along the root axis transport of each ionic form predominates. We have, therefore, endeavored to describe patterns of NH_4^+ and NO_3^- uptake along the apical 7 cm of 7-d-old intact barley roots. At this stage of development, the different anatomical regions have reached their maximum longitudinal separation along the root axis (31).

Previous techniques developed to study ion uptake along the root axis have virtually all relied on the use of isotopic tracers or an element such as bromine that is generally absent from plant tissues. Typically, after exposure to a solution containing the tracer, roots were either segmented and tissue levels of tracer determined (10), or whole roots were used for autoradiography (28, 31) or scanned with a Geiger-Müller counter (28, 31). All of these techniques measure ion accu-

---

[1] Supported in part by National Science Foundation grant DMB 87-16363, U.S. Department of Agriculture grant 88-38420-3836, and funds provided by the Hatch Program.

Table I. *Nutrient Solutions*

Composition of nutrient solutions used in the growth and pretreatment of barley seedlings before experimental use. Concentrations are given in μM.

Salt	Solution A (1/20 MJS)	Solution B (1/20 MJS(-N))	Solution C (1/20 MJS(NH_4^+))	Solution D (1/20 MJS(NO_3^-))
KNO_3	300.0			300.0
$Ca(NO_3)_2$	200.0			
$NH_4H_2PO_4$	100.0			
K_2SO_4		150.0		
$(NH_4)_2SO_4$			150.0	
$Ca(H_2PO_4)_2$		200.0	200.0	200.0
$MgSO_4$	50.0	50.0	50.0	50.0
KCl	2.5	2.5	2.5	2.5
H_3BO_3	1.25	1.25	1.25	1.25
FeHEDTA[a]	1.0	1.0	1.0	1.0
$MnSO_4$	0.1	0.1	0.1	0.1
$ZnSO_4$	0.1	0.1	0.1	0.1
$CuSO_4$	0.025	0.025	0.025	0.025
MoO_3	0.025	0.025	0.025	0.025

[a] *N*-(2-hydroxyethyl)ethylenediamine-triacetic acid.

mulation along the root axis for the ion or analog used as a tracer. None, however, provide a dynamic view of uptake along the root because the profile produced is merely a representation of net tracer accumulation at the conclusion of the exposure period.

We have four concerns regarding previous experimental techniques and the characterizations of ion uptake along the root axis that emerge from their application: (a) the use of excised roots, (b) a nutrient-deficient regimen used to grow plants for experimentation, (c) the lack of a recovery period from movement and handling before the start of an experiment, and (d) the static representation of ion uptake along the root axis based on net accumulation of tracer. In studies in which ion uptake along the root axis is examined, each of these points strongly influences the experimental results and their interpretation. These concerns will be addressed in more detail in "Discussion."

Our experiments were based on the demonstration by Newman *et al.* (20) that net ion fluxes may be estimated from the measurement of ion activity gradients in the unstirred layer of solution immediately external to the root surface using ISMs[2]. We shall refer to this method as the MFET. It is important at this point to distinguish between the unstirred layer and the zone of ion depletion around the root; the size of the unstirred layer is determined by fluid movement around the root, whereas the zone of ion depletion is influenced both by fluid movement and by ion uptake. The zone of ion depletion is the region between the root surface and the radius at which the ion concentration reaches 99% of the bulk solution ion concentration and will hence be referred to as the diffusion boundary layer (1). The development of NH_4^+- and NO_3^--selective microelectrodes (13) has made it possible to measure NH_4^+ and NO_3^- uptake along the root axis with improved spatial and temporal resolution. Although the MFET promises to be a powerful tool for investigating ion uptake by intact roots, several important issues have not been addressed previously, including the effects of transpiration-driven bulk water flow into the root, the nature of the diffusion boundary layer, the spatial resolution, and the accuracy of the technique. An evaluation of the MFET was, therefore, conducted to clarify these points.

MATERIALS AND METHODS

Barley Culture

Germination and Growth

Barley seeds (*Hordeum vulgare* L. cv Prato) were imbibed in the dark at 28°C on germination paper moistened with 500 μM $CaSO_4$. After 24 h, germinated seeds were suspended above light-tight, 1-L containers (3M Velostat No. 4015) filled with 1/20 strength MJS (15) (Table I, solution A). This nutrient solution contained both NH_4^+ and NO_3^-, at 100 and 700 μM respectively. Each container held three seedlings, and the solutions were aerated continuously. The containers were placed in a growth chamber set for day/night temperatures of 20 and 15°C, respectively. The seedlings received light at a PPFD of 300 μmol m^{-2} s^{-1} for a 16-h photoperiod (06:00–22:00 h).

After 3 d in 1/20 strength MJS, the seedlings were transferred for 2 d into 1/20 MJS(−N) (Table I, solution B). This solution contained neither NH_4^+ nor NO_3^- but maintained equivalent concentrations of all other ions with the exception of $H_2PO_4^-$ and SO_4^{2-}, which increased from 100 to 400 μM and from 50 to 200 μM, respectively (Table I).

Pretreatment Solutions

Plants were inserted into the experimental chamber at approximately 21:30 h on the evening before the experiment.

---

[2] Abbreviations: ISM, ion-selective microelectrode; MFET, microelectrode flux estimation technique; MJS, modified Johnson's solution; MJS(−N), nitrogen-free modified Johnson's solution; MJS(NH_4^+), ammonium-based modified Johnson's solution; MJS(NO_3^-), nitrate-based modified Johnson's solution; emf, electromotive force.

A particular pretreatment solution was circulated through the chamber for approximately 12 h, until the start of the experiment the following morning. In the case of NH_4^+ axial scans, the pretreatment solution was 1/20 MJS(−N) (Table I, solution B). This was to ensure that at the start of the experiment plants would take up NH_4^+ at a significant rate. Although some reports have appeared suggesting that NH_4^+ uptake may be substrate inducible (9), our experiments have failed to show that pretreatments with NH_4^+ are necessary for significant initial rates of NH_4^+ uptake. In contrast, to be able to distinguish between changes in net NO_3^- flux due to axial position *versus* changes in net flux due to the induction of NO_3^- uptake, the plants were exposed to NO_3^- sufficiently in advance of the start of the experiment to ensure a fully induced NO_3^- transport system (G.H. Henriksen and R.M. Spanswick, unpublished). Therefore, plants to be used for NO_3^- axial scans were pretreated for 12 h with 1/20 MJS(NO_3^-) (Table I, solution D).

Microelectrode System

Microelectrode System Improvements

Several modifications were made to the experimental system (Fig. 1) previously described (13). The shoot was illuminated using two low voltage lamps (Wild HeerBrugg Ltd., model 1052) giving a PPFD of 150 μmol m^{-2} s^{-1} perpendicular to the leaf surface. This configuration prevented illumination of the root system, as well as inadvertent heating of the solution in the experimental chamber and subsequent temperature-dependent variations in microelectrode response (13). In addition, light levels were kept low to minimize transpiration and consequent ion uptake due to bulk water flow (see "MFET Theory").

A brass, telescoping (4–6 cm), signal-driven shield was extended over the microelectrode holder and the shaft of the microelectrode itself, to within 5 mm of the solution surface. The stainless steel experimental chamber (Fig. 2; 13, fig. 1) was connected directly to the chassis ground of the electrometer, as was a braided wire shield surrounding the cable between the motor-driven micromanipulator (Märzhäuser, model DC-3K) and its control panel. These modifications dramatically improved the signal to noise ratio and, in conjunction with the addition of a 10 μV-resolution digital multimeter (Keithley Instruments, model 175) connected to the differential output of the dual electrometer (World Precision Instruments, model FD223-G), improved the accuracy of the MFET.

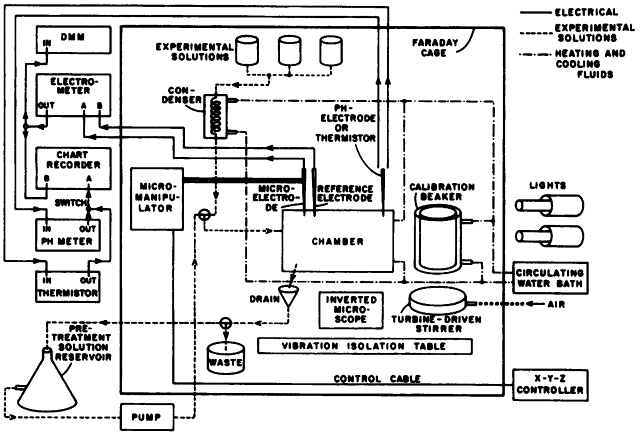

Figure 1. Schematic of microelectrode system. Elements in the system used to measure net ion fluxes into roots using ISMs in the unstirred layer of solution immediately external to the root surface.

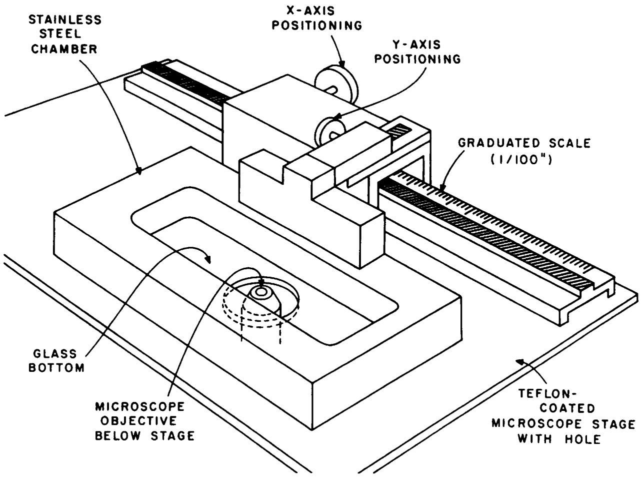

Figure 2. Detail of rack and pinion positioning system. Chamber position, and thus root position with respect to the microelectrode tip, was adjusted by means of a rack and pinion mechanism.

A 30.5-cm-long rack and pinion slide with an associated platform (Edmund Scientific Co., Nos. F31 and 241 and Nos. F31 and 240) was attached to the stainless steel chamber, allowing the chamber to be moved along the x and y axes to facilitate positioning of the microelectrode tip along a 10-cm length of root (Fig. 2). To reduce friction during chamber movement, both the steel portion of the chamber bottom and the stage of the inverted microscope were covered with Teflon pressure-sensitive sheeting (Scientific Specialties, Randallstown, MD; No. S32510). A scale on the rack with 0.01-inch (0.254 mm) graduations provided a means to return reliably to axial positions at which measurements had previously been made. Unique features along the root surface visible at high magnification were also found to be useful in returning to previous measurement positions.

Finally, the solution delivery system was modified to include a loop whereby a pretreatment solution could be cycled through the experimental chamber (Fig. 1). The addition of a peristaltic pump (Harvard Apparatus model 1201), in line with a 3-L reservoir, enabled a particular pretreatment solution to be circulated through the chamber at a flow rate of 50 mL min^{-1} for at least 12 h before the start of the experiment the following morning. The benefits of this arrangement were twofold: the plant had ample time to recover from movement and handling (3) and a nutrient solution pretreatment could be administered in advance of experimental measurements.

Microelectrode Fabrication

NH_4^+- or NO_3^--selective microelectrodes were fabricated in groups of eight the evening before an experiment as described previously (13). In brief, micropipets were pulled from 2.0-mm, o.d., capillary blanks and then silanized for 5 min on the surface of a hot plate. After the micropipets were back-filled with an appropriate solution, they were front-filled with either NH_4^+- or NO_3^--selective liquid ion-exchange resin and then stored overnight tip down in a solution similar to that used for back-filling. On the following morning, several microelectrodes were tested, and the best was selected for calibration. Selection was based on a combination of three factors: slope (mV $decade^{-1}$), drift (mV min^{-1}), and response time.

Microelectrode Calibration

Once selected, the microelectrode was calibrated between 50 and 1000 μM in the following sequence: 50, 100, 200, 500, and 1000 μM. Calibration solutions consisted of 200 μM $CaSO_4$, 1.1 mM $MgSO_4$ to adjust the ionic strength to approximately 4.4 mM, and the ion of interest added in small aliquots as either $(NH_4)_2SO_4$ or $Ca(NO_3)_2$. A similar calibration was performed at the conclusion of the experiment. Linear regressions were calculated for each calibration curve and the regression coefficients compared to determine whether the microelectrode response had changed significantly during the course of the experiment. The difference between the slope values from the initial and final calibration regression equations constituted one component in the calculation of the total MFET uncertainty (see "MFET Accuracy Estimation"). This difference was never observed to exceed 1 mV $decade^{-1}$, corresponding to an inaccuracy in the net flux calculation of <0.1% (from Eq. 24). Therefore, the initial and final electrode slopes were averaged when calculating ion concentrations from emf readings.

Although it is not possible to ensure against microelectrode drift during the course of the experiment, it is possible to compensate for electrode drift when calculating ion concentrations from emf readings. This was done by recalculating the intercept of the regression equation each time the microelectrode tip was repositioned in the bulk solution; the underlying assumption is that the bulk solution concentration remains virtually constant during the 90 min between solution changes. This assumption was verified by removing aliquots of solution from the experimental chamber at the beginning and end of several 90-min periods and measuring their NO_3^- concentration with a NO_3^--selective macroelectrode (Orion, model 93–07). A t test with 95% confidence limits revealed no significant difference in NO_3^- concentration between the two groups of samples.

Experimental Protocols

Transpiration Experiments

Because bulk water movement toward the root surface affects MFET results (see "MFET Theory"), experiments were conducted to estimate typical transpiration rates. Root systems of intact 7-d-old seedlings were inserted into 50-mL Erlenmeyer flasks containing experimental solution. The seedlings were supported by foam plugs around the caryopsis and sealed into the flasks with high vacuum silicone grease (Dow Corning). Flasks containing plants were weighed with a digital analytical balance (Fisher, model XA100) before placement under environmental conditions identical with those experienced by the plants during MFET experiments. The PPFD at the leaf surface was 150 μmol m^{-2} s^{-1}, the ambient temperature was 23.6 ± 0.2°C, and the RH (40.5 ± 3.0%) was determined using a sling psychrometer. Weights were recorded at 15-min intervals during the course of 2 h, and weight loss was plotted as a function of time. Weight loss was found to be linear with time ($r^2 > 0.99$), and it was assumed that weight loss was due only to transpiration. This assumption was supported by control experiments performed on flasks without plants. At the conclusion of the experimental period, root and shoot lengths were estimated, and root fresh and dry weights were measured. Transpiration rates based on root surface area (L m^{-2} s^{-1}) were then calculated.

Net Ion Flux Measurements

Net ion flux experiments were begun after the plants had been exposed to the pretreatment solution for 12 h. At the start of an experiment, solution was allowed to flow into the experimental chamber (130 mL volume) for 15 min at a rate of 70 mL min^{-1}. For NH_4^+-based experiments, the solution consisted of 100 μM $(NH_4)_2SO_4$, 200 μM $CaSO_4$, and 1.1 mM $MgSO_4$. When the ion of interest was NO_3^-, the solution contained 100 μM $Ca(NO_3)_2$, 100 μM $CaSO_4$, and 1.1 mM $MgSO_4$. After the solution inflow was stopped, a period of 2 to 3 min was permitted for electrode settling before an emf reading was taken in the bulk solution. The microelectrode tip was then moved in a direction perpendicular to the root axis along a radius (Fig. 3). The tip of the microelectrode was positioned at 100, 50, 25, 50, and 100 μm from the root surface using the motor-driven micromanipulator and a calibrated eyepiece reticle; an emf reading was made at each position. After the second reading at 100 μm, the tip was moved back into the bulk solution, and a final emf reading was taken to complete one cycle of ion concentration measurements. The temporal resolution of the MFET (approximately 15 s) is the sum of both the time necessary for tip movement between positions (approximately 10 s) and the

Figure 3. MFET. The MFET uses activity (concentration) measurements (c_1 and c_2) in the unstirred layer of solution to calculate net ionic fluxes at the root surface (J_{root}). D^{*o} is the self-diffusion coefficient of the ion of interest. K, a units conversion coefficient, is used to express J_{root} in units of nmol m^{-2} s^{-1}. Ion concentrations are measured at two radial distances (r_1 and r_2) from the root center. The root radius is given by r_{root}.

time required for the electrode to respond to a change in ion concentration (approximately 5 s).

It is possible to improve MFET accuracy by using ion concentration measurements at more than two locations to arrive at an estimate of net ion flux. In this method, measurements at several positions are used in a linear regression; the slope of the regression line is then used to calculate the net ion flux (see "MFET Theory"). However, this improvement is only realized if electrode drift is low and root uptake rates are relatively constant over time. To minimize the influence of electrode drift, and because fluctuations in ion uptake were observed within relatively short periods, we chose to use pairs of measurements closely spaced in time. In-going measurements made at 100- and 50-μm positions were paired, as were out-going measurements at 50 and 100 μm, so that each cycle of measurements yielded two estimates of the net ion flux into the root.

The rack and pinion slide (Fig. 2) was used to reposition the chamber so that net flux estimates were obtained at five locations along the apical 7 cm of root. These five cycles of measurements were completed within 90 min and were followed by a 12-min flushing of the chamber with fresh experimental solution before beginning the next set of measurements. Four such 90-min measurement periods constituted a complete experiment.

MFET Theory

The MFET uses ion activity measurements (equivalent to concentration in dilute solutions), taken at several positions in the diffusion boundary layer, to estimate the net flux[3] of ions (J) into the root. The conversion of concentration gradient data into flux estimates requires assumptions about the mechanisms of ion transport to the root surface and the nature of the diffusion boundary layer, as well as the geometry of the root; different assumptions yield different flux estimates from the same data. We shall first derive the relationship between flux and concentration gradients for three cases and then use experimental observations to choose the case that best describes the conditions in our experimental system. In all three cases, we make the following simplifying assumptions: roots exhibit morphological and physiological cylindrical symmetry, and uptake is constant along an infinite length of root. Although this second assumption is clearly violated in real root systems, it will be shown that a relatively short (approximately 1.0 mm) length of root may be treated as an infinite cylinder.

Ion movement in the diffusion boundary layer can be due to gradients in electrochemical potential or due to the transpiration-driven movement of water into the root, hereafter referred to as bulk flow. The emf of an ion-selective electrode will be due to both the activity of the ion of interest and any electrical potential differences in solution. It is, therefore, important to determine whether significant electric fields are occurring in the unstirred layer and contributing to the measured emf. The electric field component of the total electrochemical potential gradient was estimated and found to be negligible when compared to the concentration component. This estimate was based on reported values for ion current densities (2 μA cm^{-2}) around barley roots (30) and the specific conductivities of our experimental solutions (approximately 300 μS cm^{-1}). Therefore, the two transport mechanisms responsible for ion movement toward the root surface are diffusion, driven by the concentration gradient, and bulk flow. Diffusion driven by a concentration gradient is termed ordinary diffusion (1) and will be the only type of diffusion considered in this paper.

Root geometry may be approximated by a cylinder, with ion flux assumed to be in the radial direction only. The area (A_s) over which the flux occurs is, therefore, $2\pi rl$, where r is the radial distance (m) from the root center and l is the root length. For steady-state uptake, ion flow into the root (ϕ, mol s^{-1}) is constant. Because flux (J, mol m^{-2} s^{-1}) is flow per area, flux is inversely proportional to r. This is in contrast to the case of planar diffusion, where A_s remains constant along the paths of the diffusing ions. Under certain limited experimental conditions, planar diffusion may be an adequate approximation of the cylindrical diffusion that is actually occurring; however, such an approach lacks rigor and always introduces some error (see Eq. 9). Alternatively, cylindrical coordinates yield correct results regardless of root size and measurement location.

In contrast to flux, flow is independent of radial position under steady-state uptake conditions, making it advantageous to compute flow from concentration gradient data. Flow can be converted to flux at the root surface by the following equation: $J_{root} = \phi/A_{s(root)}$, where the root surface area, $A_{s(root)}$, is given by $2\pi r_{root}l$, where r_{root} is the root radius. Alternatively, flow per unit root mass (mol g fresh weight^{-1} s^{-1} or mol g dry weight^{-1} s^{-1}) can be computed if the root fresh or dry weight is known (20). To simplify the following derivations, flow is expressed on a unit length basis (ϕ_l, mol m^{-1} s^{-1}), and influx is defined as positive and efflux as negative.

Case 1: Diffusion Only, Constant Diffusion Boundary Layer

We will first consider conditions similar to those used by Newman *et al.* (20) in their derivation, which allow for a constant diffusion boundary layer and ordinary diffusion as the only driving force for ion movement toward the root. This is described by Fick's First Law, which expresses the proportionality between flux and concentration gradient:

$$J = D^{*o}\frac{\partial c}{\partial r}, \tag{1}$$

where D^{*o} is the self-diffusion coefficient (m^2 s^{-1}), and c is the concentration (mol m^{-3}). The minus sign normally found is omitted because, in uptake measurements, influx is defined as positive. Under steady-state conditions, the law of conservation of mass dictates that the amount of matter entering a volume must be equal to the amount leaving the volume; in the cylindrically symmetric case, this constraint has the following expression (1):

---

[3] Following standard engineering terminology, we will use "flux" strictly to mean the amount of material passing through a unit area per unit time (mol m^{-2} s^{-1}).

$$J + r\frac{\partial J}{\partial r} = 0, \tag{2}$$

Substitution of Equation 1 into Equation 2 yields the differential equation for steady-state radial diffusion in a cylindrical system:

$$\frac{\partial^2 c}{\partial r^2} + \frac{1}{r}\frac{\partial c}{\partial r} = 0. \tag{3}$$

It is easily verified that the general solution to Equation 3 is:

$$c = \beta_1 \ln(r) + \beta_2, \tag{4}$$

where β_1 and β_2 are constants determined by the boundary conditions. At the root surface, where flux is known to be the flow (ϕ_l) divided by the root surface area per unit root length, the boundary condition is given by:

$$J_{root} = \frac{\phi_l}{2\pi r_{root}} = D^{*o}\left(\frac{\partial c}{\partial r}\right)_{r = r_{root}}. \tag{5}$$

Substituting Equation 4 into Equation 5 and rearranging gives:

$$\phi_l = 2\pi D^{*o}\beta_1. \tag{6}$$

Equation 4 implies that concentration (c) changes linearly with the natural logarithm of radius. If c is plotted against $\ln(r)$ (Fig. 4), the slope of the line will be β_1, which can be calculated from two points as:

$$\beta_1 = \frac{c_2 - c_1}{\ln(r_2/r_1)}. \tag{7}$$

Substituting Equation 7 into Equation 6 yields:

$$\phi_l = 2\pi D^{*o}\frac{c_2 - c_1}{\ln(r_2/r_1)}. \tag{8}$$

Equation 8 can be used to estimate flow using concentration measurements at two radial positions. This will be referred to as the two-point MFET. For convenience, a shorthand notation indicating the inner and outer distances from the root surface will be used in this paper; *e.g.* 50/100 MFET indicates the two-point MFET with measurements made 50 and 100 μm from the root surface. If more than two locations are sampled, a least squares fit of the concentration (c) as a function of $\ln(r)$ yields β_1 as the slope and β_2 as the y intercept, where $\ln(r) = 0$ (Fig. 4). Although β_2 has no direct physical significance, if both β_2 and β_1 are known, they can be used to calculate the root surface concentration and the approximate size of the diffusion boundary layer. Notice that flow, the variable of interest, is completely determined by the slope of the c *versus* $\ln(r)$ line; finding the second constant of integration (β_2) is unnecessary for the MFET.

An expression for the error in net flux calculations incurred by assuming that planar diffusion is occurring in a cylindrical system can be derived using Equations 1, 4, 5, and 6. Only the result is presented below:

$$\%\text{error} = 100\left(1 - \frac{r_{root}\ln(r_2/r_1)}{r_2 - r_1}\right). \tag{9}$$

Substituting typical values for r_{root} of 225 and 500 μm for barley and maize, respectively, the use of planar diffusion coordinates for the 50/100 MFET will result in a 25% error in the net flux calculation for barley, and a 13% error in the flux calculation for maize. If a 20/60 MFET is used with a maize root (24), the error in the flux calculation will be 7%. Inasmuch as other elements in the MFET introduce varying amounts of error into the calculation of net ion fluxes (see "MFET Accuracy Estimation"), the addition of another source of error through the inappropriate use of planar diffusion equations is unnecessary and easily avoided.

Case 2: Diffusion and Bulk Flow, Constant Diffusion Boundary Layer

We will now assume that ion movement due to ordinary diffusion occurs in conjunction with ion movement due to a radial flow of water into the root so that Fick's First Law must be amended with a term representing ions moving with the bulk flow of water. This can be done by multiplying $J_{w(v)}$, the volumetric water influx ($m^3\ m^{-2}\ s^{-1}$), by the concentration of the ion in solution (1):

$$J = D^{*o}\frac{\partial c}{\partial r} + J_{w(v)}c. \tag{10}$$

The mathematical expression of mass conservation remains the same; therefore, substitution of Equation 10 into Equation 2 yields the differential equation for steady-state radial diffusion and bulk flow in a cylindrical system:

$$\frac{\partial^2 c}{\partial r^2} + (1 + k_w)\frac{1}{r}\frac{\partial c}{\partial r} = 0, \tag{11}$$

$$\text{where } k_w = \frac{J_{w(v)root}r_{root}}{D^{*o}}$$

and $J_{w(v)root}$ is the volumetric water influx at the root surface. The general solution to this equation for non-zero k_w is:

$$c = \beta_3 r^{-k_w} + \beta_4, \tag{12}$$

where β_3 and β_4 are constants determined by the boundary conditions. By applying the surface flux boundary condition, as was done in case 1, the relationship between these constants and the uptake rate is found. These constants can be determined by a linear regression on two or more data points and then used to compute flux and flow. The two-point flow formula is given here:

$$\phi_l = 2\pi r_{root}J_{w(v)}\left(c_2 - \frac{r_2^{-k_w}(c_2 - c_1)}{r_2^{-k_w} - r_1^{-k_w}}\right). \tag{13}$$

If zero bulk flow is assumed, even though significant transpiration is actually occurring, the percentage error in the estimated flux incurred by using Equation 8 instead of Equation 13 is given by:

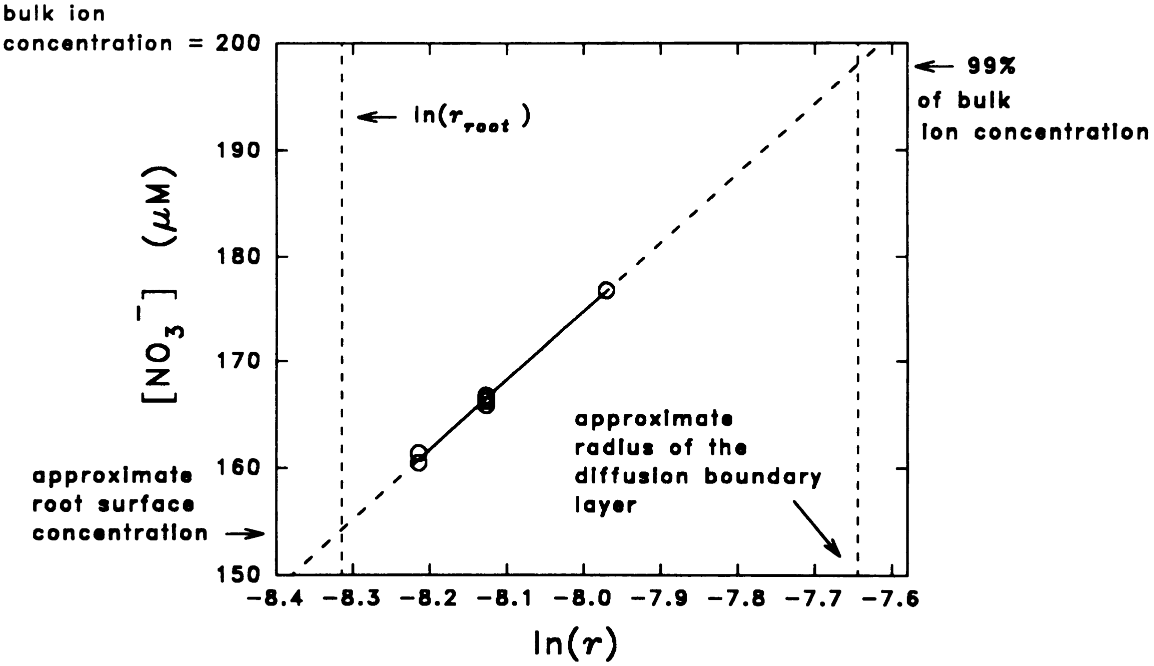

Figure 4. Relationship between c and $\ln(r)$. The result of a linear regression is drawn through data from a typical cycle of concentration measurements. Points of intersection may be used to estimate the concentration at the root surface, as well as the radius of the diffusion boundary layer. In this instance, the radius of the diffusion boundary layer was approximately 500 μm. The root surface $[NO_3^-]$ was approximately 155 μM. The units for r are meters.

% error =

$$100\left(1-\frac{D^{*o}}{r_{root}J_{w(v)root}\ln(r_2/r_1)\left(\frac{c_2}{c_2-c_1}-\frac{r_2^{-k_w}}{r_2^{-k_2}-r_1^{-k_w}}\right)}\right). \quad (14)$$

Substitution of values into Equation 14 reveals that the percentage error becomes larger as the solution concentration increases. This is expected because more of the ion is carried per unit water flow when the concentration is higher. If measurements are attempted in high solution concentrations, two methods may be used to minimize the error; either transpiration should be quantified so that $J_{w(v)root}$ is known and Equation 13 can be used, or transpiration should be reduced so that use of Equation 8 results in insignificant errors.

Case 3: Diffusion Only, Time-Varying Diffusion Boundary Layer

We now remove our previous constraint concerning constant diffusion boundary layer size. The governing differential equation in this case is:

$$\frac{\partial^2 c}{\partial r^2}+\frac{1}{r}\frac{\partial c}{\partial r}=\frac{1}{D^{*o}}\frac{\partial c}{\partial t}. \quad (15)$$

The two boundary conditions are: (a) constant flux at the root surface, a condition that is reasonable in light of the fact that the bulk solution concentration is more than an order of magnitude larger than the K_m for both NO_3^- and NH_4^+ (11), and (b) a constant concentration in the solution far away from the root. The necessity of the vague term "far away from" arises because the diffusion boundary layer size is variable; initially, the entire solution is at constant concentration and there is no diffusion boundary layer. As time (t) progresses, ion uptake causes a zone of depletion to form; in a completely motionless fluid, this zone grows indefinitely. Mathematically, the second boundary condition is expressed as $c \rightarrow c_0$ as $r \rightarrow \infty$, where c_0 represents the bulk solution concentration. In addition to the two boundary conditions, an initial condition is required for the solution of the time-dependent equation. This initial condition is that at $t = 0$, $c = c_0$ everywhere in the fluid. These boundary and initial conditions, along with Equation 15, are analogous to those describing the temperature distribution around a cylindrical heat source in an unbounded material. Carslaw and Jaeger (5) found a solution to this equation that is fairly complex. However, they present a simplified solution, valid for $t >> (r)^2/D^{*o}$. At 20°C, values of D^{*o} for NH_4^+ and NO_3^- have previously been calculated to be 1.74×10^{-9} and 1.67×10^{-9} $m^2\ s^{-1}$, respectively (13). Therefore, when making measurements 100 μm from the surface of a root of 225 μm radius, $(r)^2/D^{*o} \approx 120$ s. The simplified solution is, therefore, legitimate for all but the first few minutes of the 90-min measurement period. Making the appropriate conversions between Carslaw and Jaeger's heat transfer solution and the mass transfer problem of interest yields:

$$c = c_0 + \frac{\phi_l}{2\pi D^{*o}}\left[\ln(r) - \ln(\sqrt{t}) - \ln(\sqrt{D^{*o}/e^{\gamma}})\right], \quad (16)$$

where $\gamma = 0.57722$ (Euler's constant). The first term in the brackets indicates that the positional variation of concentration is identical with that given in Equation 4, whereas the second term addresses the temporal change in concentration due to the depletion of the solution around the root. It is possible to determine whether or not the solution is being depleted, as predicted by Equation 16, by comparing the concentration profiles at different times.

RESULTS

MFET Evaluation

To maximize the accuracy of the MFET, an equation appropriate to the experimental conditions must be used to convert concentration gradient data into flux estimates. Having explored the relationship between flow and concentration gradients for three sets of conditions, we will now choose the case that best describes the conditions observed in our experimental system. In so doing, we will determine the appropriate equation to be used in calculating net ion fluxes, then develop an estimate of the spatial resolution of the MFET, and finally generate an expression for calculating the uncertainty inherent in making measurements of this type.

As explained in the MFET theory, concentration data may be used to estimate the size of the diffusion boundary layer (Fig. 4). We have observed experimentally that diffusion boundary layers do not increase steadily with time; rather, they are fairly constant. This phenomenon is not expected in a perfectly still fluid; Equation 16 suggests that the zone of depletion increases steadily around a root that is removing ions from solution. The large, fixed diffusion boundary layers that we observe imply that small convection currents exist in our experimental chamber. This is likely to be due to minor temperature gradients between the surface of the experimental solution and the chamber walls, which are maintained at 20°C. Because we observed a fixed diffusion boundary layer, we concluded that our experimental system would be modeled best by the application of equations developed in case 1 or case 2 (see "MFET Theory").

Two equations were developed for conditions of a fixed diffusion boundary layer; one describes the case wherein only diffusion is responsible for ion movement to the root, and the other considers the effects of both diffusion and bulk flow in transporting ions to the root. If transpiration is quantified, then Equation 14 may be used to assess the error incurred in applying Equation 8, which ignores the contribution of transpiration-driven bulk water flow. To this end, experiments were performed to estimate the bulk flow of water into the root.

Transpiration experiments indicated a maximum $J_{w(v)root}$ of 1.4×10^{-5} L m^{-2} s^{-1} when averaged over the entire root surface. Applying this value in Equation 14 yields a prediction of a typical error of 0.6% in our experimental solutions in which the concentration of the ion of interest was 200 μM. The predicted error would increase to 5.5% if the local $J_{w(v)root}$ were an order of magnitude greater than the average values, an unlikely condition, even though it has been shown that water uptake is not uniform over the entire root surface (26). The effect of bulk flow was, therefore, considered to be insignificant, and Equation 8, rather than Equation 13, was used to calculate net ion flow. Net ion flux (J_{root}) at the root surface can be computed by dividing Equation 8 by root surface area per unit length ($2\pi r_{root}$):

$$J_{root} = \frac{KD^{*o}}{r_{root}} \frac{c_2 - c_1}{\ln(r_2/r_1)}, \tag{17}$$

where K is a units conversion coefficient. Having chosen the equation that best describes the conditions observed with our experimental system, we will next develop an estimate of the spatial resolution of the MFET.

Axial Variations in Uptake and the Spatial Resolution of the MFET

Axial variations in uptake influence the direction of ion flow by adding an axial (z direction) diffusion component to the radial component. To investigate the spatial resolution of the MFET, we will model a hypothetical situation in which the root surface flux (J_{root}) is constant along a segment of root and zero along adjacent segments (Fig. 5). If we assume a constant diffusion boundary layer, the governing differential equation becomes:

$$\frac{\partial^2 c}{\partial r^2} + \frac{1}{r}\frac{\partial c}{\partial r} + \frac{\partial^2 c}{\partial z^2} = 0. \tag{18}$$

As with the time-varying case (case 3), a heat transfer analogy exists and has been solved by Carslaw and Jaeger (5).

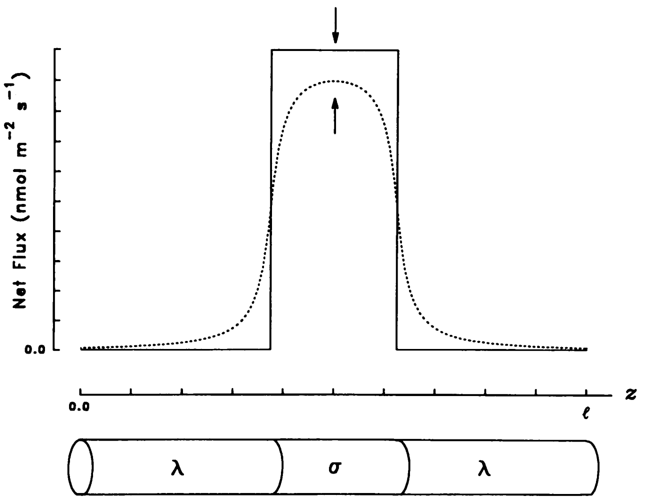

Figure 5. Spatial resolution modeling. The region of length σ, centered on a root segment of length l, represents a zone of constant uptake; the regions of length λ on either side represent zones of zero uptake. The solid line represents the hypothetical root surface flux; the dashed curve depicts the result of a computer simulation of the flux as determined by the MFET, using Equation 17. Of particular interest in determining the spatial resolution of the MFET is the difference (see arrows) between the actual root surface flux and the flux determined by the MFET at the axial position centered on σ.

The appropriately transformed result is given as:

$$c = \frac{4J_{root}l}{D^{*o}\pi^2} \times \sum_{m=0}^{\infty} \frac{F_0[(2m+1)\pi r/l;\ (2m+1)\pi b/l]\cos\alpha \sin\beta}{F_1[(2m+1)\pi a/l;\ (2m+1)\pi b/l](2m+1)^2},$$

where

$$\alpha = \frac{(2m+1)\pi\lambda}{l}, \qquad \beta = \frac{(2m+1)\pi z}{l}, \tag{19}$$

$$F_0[x;\ y] = I_0(x)K_0(y) - K_0(x)I_0(y),$$

$$F_1[x;\ y] = I_1(x)K_0(y) + K_1(x)I_0(y),$$

$$\lambda = \frac{l-\sigma}{2},$$

and where a and b represent the radius of the root and diffusion boundary layer, respectively, z represents the axial distance from the end of the segment, l represents the root length, σ is the length of the root segment showing constant uptake, and λ represents the lengths of root segments having zero uptake; I_n and K_n are modified Bessel functions of the first and second kind, order n. Equation 19 was implemented on a computer, using subroutines to compute the Bessel functions (22) so that concentrations at any location ($0 < z < l$, $a < r < b$) could be calculated. The following values were used: J_{root}, 500 nmol m^{-2} s^{-1}; l, 30 mm; a, 0.225 mm; b, 0.725 mm; D^{*o}, 1.7×10^{-9} m^2 s^{-1}; and σ, varied from 0.01 to 1.0 mm. The concentrations calculated by the program were substituted into Equation 17 so that the flux value that a two-point MFET would yield could be calculated and compared with the actual root surface flux (J_{root}).

Figure 6 shows a graphical representation of such a comparison. Notice that as the width (σ) of the constant uptake segment is increased, the MFET results provide a better estimate of the actual root surface flux; when σ is 0.84 mm, the 50/100 MFET reads 95% of the true value of the root surface flux. We have chosen this value of σ (0.84 mm) as representative of the spatial resolution of the 50/100 MFET, because other system elements limit the accuracy of the MFET to approximately 95% (see "MFET Accuracy Estimation").

It is apparent from Figure 6 that the spatial resolution improves as the measurements are made closer to the root; the 10/20 MFET measures 95% of the actual root surface flux when σ is only 0.27 mm. However, improved spatial resolution comes at the cost of increased measurement uncertainty, as demonstrated in the following section.

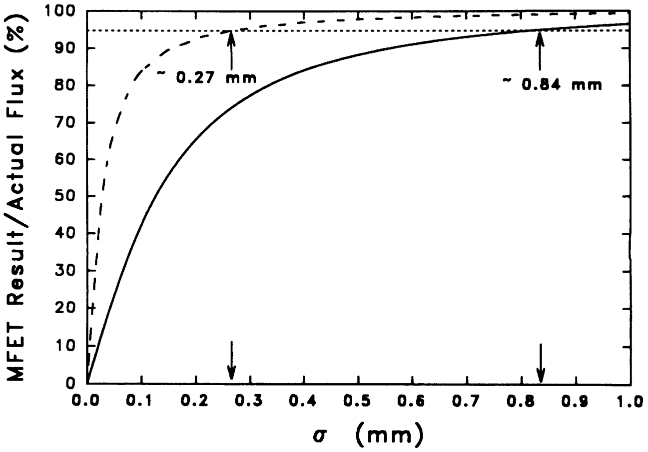

Figure 6. Spatial resolution modeling. The width of the constant flux segment, σ, determines the accuracy of the MFET; the axial position of the microelectrode is centered on the root segment. The width (σ) of the segment exhibiting constant uptake was varied from 0.01 to 1.0 mm, in steps of 0.01 mm. The MFET estimation of the root surface flux is described as a percentage of the actual root surface flux and is a function of σ. The solid line represents the 50/100 MFET; the dashed line represents the 10/20 MFET. Note that, as σ increases, the flux estimate yielded by the MFET approaches the actual root surface flux. When σ is 0.84 mm, the 50/100 MFET reading is 95% of the actual root surface flux. The 10/20 MFET reads 95% of the actual root surface flux when σ = 0.27 mm. The gain in spatial resolution achieved by measuring close to the root surface comes at the cost of an increase in the uncertainty of the measurement (see "MFET Accuracy Estimation").

MFET Accuracy Estimation

Although it is desirable to find an estimate of the accuracy of the MFET, an appropriate approach has yet to be described. Several common techniques for determining measurement accuracy cannot be used for the MFET; a cylindrical device with a constant, known uptake rate is not available as a calibration standard and performing a statistical analysis on a group of measurements is also problematic because it is not possible to know whether to attribute variations in MFET results to measurement errors or to changes in flux. However, each of the components used in the net flux calculation has a measure of uncertainty associated with it. It is possible to determine, by assessing the uncertainties in the component measurements, the accuracy of the net flux estimate. It is necessary to decide on the level of confidence desired in the accuracy limits when making such an assessment. We have chosen the conservative level of 95% confidence for the accuracy calculations, meaning that the value produced by the MFET will be within the calculated accuracy limits 95% of the time.

Kline and McClintock (16) showed that the best method for combining component uncertainties, to arrive at an estimate of the overall system uncertainty, depends on the way in which the uncertainty is expressed. If N represents a derived quantity, which is a function of several independent variables $u_1, u_2, \ldots u_k$, and if δu_j represents the experimentalist's confidence that some portion (*e.g.* 95%) of the measurements will fall within the range $u_j \pm \delta u_j$, Kline and McClintock (16) found that δN, the uncertainty in N that corresponds to the same confidence interval, is given by:

$$\delta N = \sqrt{\sum_{j=1}^{k} \left(\delta u_j \frac{\partial N}{\partial u_j}\right)^2}. \tag{20}$$

Notice that the uncertainty in any independent variable (δu_j) is scaled by the differential change in N for a change in u_j. To use Equation 20 to estimate the accuracy of the MFET, ϕ_l will be expressed in terms of measurable variables (u_j).

The concentration terms in the two-point MFET are computed from the electric potentials measured across the ISM/reference electrode circuit, according to the following expression that is easily derived from the Nernst equation:

$$c_1 = c_0 10^{((E_1 - E_0)/m)}. \tag{21}$$

In this equation, concentrations have been substituted for ion activities, a valid conversion when solutions are dilute and the activity coefficient is essentially unity. It has also been assumed, based on the estimation of the electrical potentials around the root, that the measured emf is entirely due to the chemical potential of the ion of interest across the microelectrode liquid membrane. In Equation 21, m represents the slope (mV decade^{-1}) of the electrode response, and is determined during calibration experiments, and E_0 is the electrode response to c_0, the bulk solution concentration.

Substituting these expressions into Equation 8 gives:

$$\phi_l = c_0 D^{*o} \frac{10^{((E_2 - E_0)/m)} - 10^{((E_1 - E_0)/m)}}{\ln(r_2/r_1)}. \tag{22}$$

Equation 22 gives ϕ_l as a function of the measurable quantities E_0, E_1, E_2, r_1, r_2, and m, whose uncertainties can be estimated. Equation 20 is then applied to find the uncertainty in ϕ_l as a function of the component measurement uncertainties:

$$\begin{aligned}\delta\phi_l = \phi_l \Bigg[& \left(\frac{2.3\ \delta E_0}{m}\right)^2 + \left(\frac{2.3\ \delta E_1 c_1}{m(c_2 - c_1)}\right)^2 + \left(\frac{2.3\ \delta E_2 c_2}{m(c_2 - c_1)}\right)^2 \\ & + \left(\frac{2.3\ \delta m}{m^2}\left(E_0 + \frac{E_2 c_2 - E_1 c_1}{c_2 - c_1}\right)\right)^2 \\ & + \left(\frac{\delta r_1}{r_1 \ln(r_2/r_1)}\right)^2 + \left(\frac{\delta r_2}{r_2 \ln(r_2/r_1)}\right)^2 \Bigg]^{1/2}.\end{aligned} \tag{23}$$

This is further simplified because we estimate equal uncertainties in the emf terms ($\delta E_0 = \delta E_1 = \delta E_2 = \delta E$) and in the positioning terms ($\delta r_1 = \delta r_2 = \delta r$):

$$\begin{aligned}\delta\phi_l = \phi_l \Bigg[& \left(1 + \frac{c_2 + c_1}{c_2 - c_1}\right)\left(\frac{2.3\,\delta E}{m}\right)^2 + \left(\frac{2.3\,\delta m}{m^2}\right)^2 \\ & \left(E_0 + \frac{E_2 c_2 - E_1 c_1}{c_2 - c_1}\right)^2 + \left(\frac{1}{r_2{}^2} + \frac{1}{r_1{}^2}\right)\left(\frac{\delta r}{\ln(r_2/r_1)}\right)^2 \Bigg]^{1/2}.\end{aligned} \tag{24}$$

Notice that the fractional uncertainty ($\delta\phi_l/\phi_l$) is simply the term in square brackets in Equation 24. Net ion flux (J) is related to flow (ϕ_l) through r_{root} (Eq. 5). Because the uncertainty in determining r_{root} is negligible (approximately ±0.7%), the uncertainty in net flux, δJ, can be found simply by multiplying J by the fractional uncertainty. As shown earlier, spatial resolution improves as concentration measurements are made closer to the root surface. However, this results in large uncertainties in the calculated flux because $r_2/r_1 \rightarrow 1$, which drives $\ln(r_2/r_1) \rightarrow 0$, and thus drives the entire term $[\delta r/\ln(r_2/r_1)]$ in Equation 24 to large values.

In summary, we have determined that our experimental system is best described by equations based on the assumption that the diffusion boundary layer remains relatively constant and that ions move primarily by diffusion. Having established that Equations 8 or 17 are appropriate, we determined the spatial resolution of the 50/100 MFET to be 0.84 mm and derived Equation 24 to determine the uncertainty in the net flux estimates.

Axial Scan Experiments

It was experimentally observed that the diffusion boundary layer does not change appreciably during a cycle of measurements. This permitted the use of Equation 8, which was based on the assumption of constant diffusion boundary layer size. To determine the overall uncertainty associated with net ion flux estimates, it was necessary to assess the uncertainties in (a) positioning the microelectrode tip, (b) determining the emf, and (c) the slope of the microelectrode response. Limitations in optical resolution caused us to estimate the uncertainty in radial positioning of the electrode tip as ±2.0 μm, whereas observation of the digital multimeter display led us to estimate the uncertainties in emf readings as ±0.02 mV. Ryan *et al.* (24) recognized that the limit of resolution of the MFET will be a function of the bandwidth of the electrical system. We determined the bandwidth of our system to be approximately 5 Hz, which predicts a thermal noise level of 0.009 mV root-mean-square. The slope uncertainty ($\pm\delta m$) was estimated for each experiment as half the difference between the slopes of the pre- and postexperiment calibration regression lines. Repeated observations have shown that the accuracy of each of these component processes is within these limits more than 95% of the time. Therefore, the actual net flux falls within the range $J \pm \delta J$ >95% of the time. Vertical error bars were used in Figures 7 through 10 to indicate $\pm\ \delta J$. Examination of the relative contributions of δE, δm, and δr to the overall uncertainty calculated using Equation 24 revealed that, in our experimental system, positioning uncertainty (δr) represents the greatest source of error; its influence on δJ is at least an order of magnitude greater than either emf or electrode slope uncertainty, δE and δm, respectively.

$NH_4{}^+$ Net Fluxes

Axial scans of net $NH_4{}^+$ uptake along the root axis revealed a significant amount of variation, both over time and among replicate plants (Figs. 7 and 8). Plants used in these experiments had been deprived of nitrogen for approximately 64 h before the start of the experiment. The net $NH_4{}^+$ flux values determined during the first hour are significantly higher than those of the subsequent three scans. It is important to note that, at each position, net $NH_4{}^+$ fluxes did not necessarily decrease consistently during the course of the four axial scans (Fig. 8). Often, a decrease followed by a significant increase in net $NH_4{}^+$ flux was observed. In several instances, neighboring zones shifted their relative magnitude of $NH_4{}^+$ uptake with respect to each other. This is evident at positions on either side of an intersection of the spline-fit lines (Fig. 7).

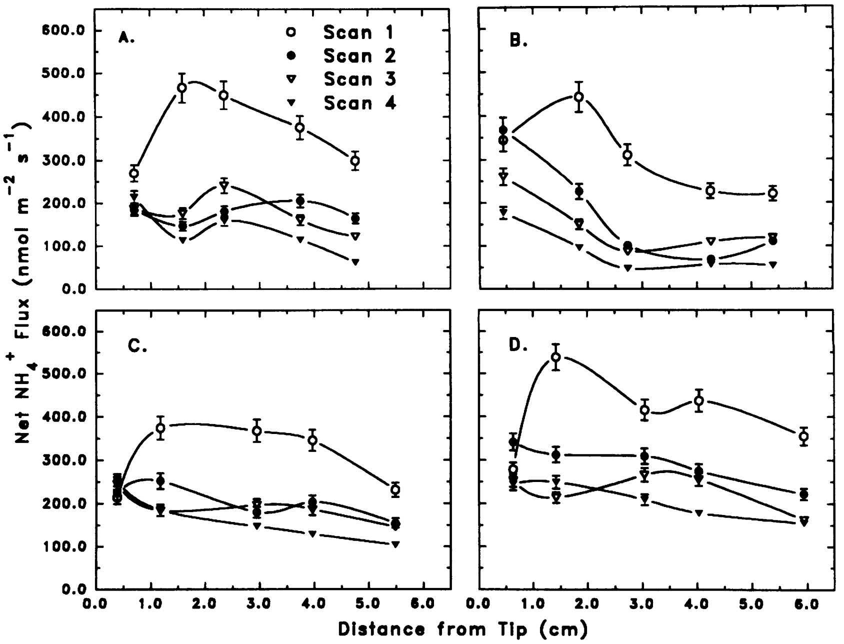

Figure 7. Variations in NH_4^+ net flux along the root axis. Axial scans of net fluxes of NH_4^+ were made at five positions along the apical 7 cm of intact, 7-d-old barley seedlings. A complete scan was made every 90 min, and four scans were conducted on each root. Each panel (A, B, C, and D) represents a single root from a different plant. Error bars represent 95% confidence based on system uncertainty calculations. The data points have been interpolated with cubic spline curves.

NO_3^- Net Fluxes

As in the case of NH_4^+ axial scans, measurements of net NO_3^- fluxes show significant variation over time and among replicate plants (Figs. 9 and 10). The high net flux values seen during the first hour of NH_4^+ uptake are absent, however; plants used for NO_3^- axial scans were given 12-h pretreatments containing NO_3^- at 300 μM and were, therefore, not nitrogen deprived at the start of the experiment. Variations in net flux at single positions were also evident during NO_3^- uptake (Fig. 10), although, as with net NH_4^+ fluxes, no particular region along the root axis appeared more subject to changes in net NO_3^- uptake than another. Again of note are points where the spline-fit lines intersect, indicating neighboring positions shifting their relative magnitudes of net NO_3^- flux (Fig. 9).

DISCUSSION

It has been demonstrated that significant reductions in both root respiration and nitrogen absorption result from excision (2, 17). Evidence suggests that reductions in ion uptake after excision have more to do with energy availability than with water flow (17, 27). In this regard, the use of intact plants

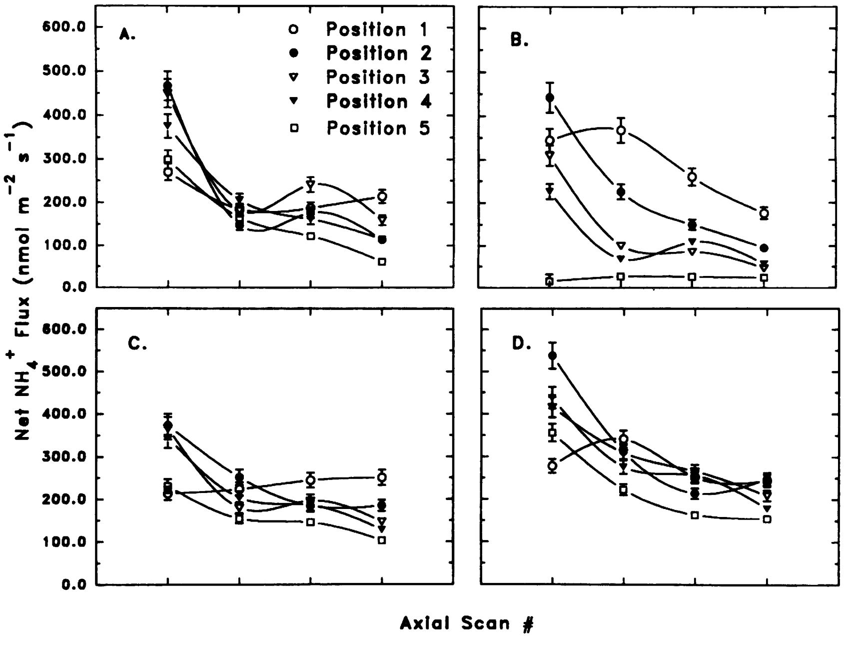

Figure 8. Variations in NH_4^+ net flux over time at each position. Axial scans of net fluxes of NH_4^+ were made at five positions along the apical 7 cm of intact, 7-d-old barley seedlings. A complete scan was made every 90 min, and four scans were conducted on each root. Each panel (A, B, C, and D) represents a single root from a different plant. Lettered panels correspond with panels in Figure 7. Error bars represent 95% confidence based on system uncertainty calculations. The data points have been interpolated with cubic spline curves.

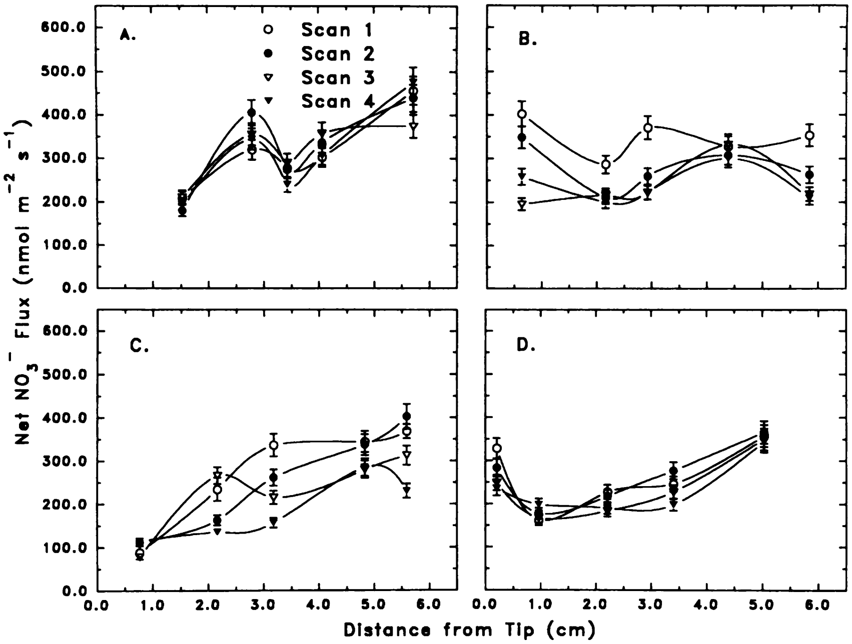

Figure 9. Variations in NO$_3^-$ net flux along the root axis. Axial scans of net fluxes of NO$_3^-$ were made at five positions along the apical 7 cm of intact, 7-d-old barley seedlings. A complete scan was made every 90 min, and four scans were conducted on each root. Each panel (A, B, C, and D) represents a single root from a different plant. Error bars represent 95% confidence based on system uncertainty calculations. The data points have been interpolated with cubic spline curves.

appears judicious when investigating aspects of root physiology pertaining to nutrient acquisition or other energy-requiring processes. Whereas the use of excised roots presents problems in the interpretation of nutrient uptake experiments, the wide variation in the nutritional status of plants used in uptake experiments poses additional difficulties. Clearly, if plants regulate mineral nutrient uptake according to their metabolic demands, their nutritional history will strongly affect the results of uptake experiments. The use of "low salt" roots in ion uptake studies is attractive because ion efflux is minimal, owing to the depleted internal storage pools of various mineral nutrients. However, inasmuch as many of the nutritional regimens designed to produce low salt roots withhold essential mineral nutrients, doubts remain as to whether this heightened uptake is representative of normal plant function. Wiebe and Kramer (31) have pointed out, however, that growing seedlings in a dilute, nutrient-complete solution will also produce roots in which ion efflux is minimal. Handling and transplant shock are further disadvantages of many of the earlier techniques; without sufficient time for the roots to recover, the uptake of ions from the external medium is reduced and perhaps altered along the root axis. Recent work by Bloom and Sukrapanna (3) has demonstrated marked and long-term reductions in both NO$_3^-$ and K$^+$ uptake by intact

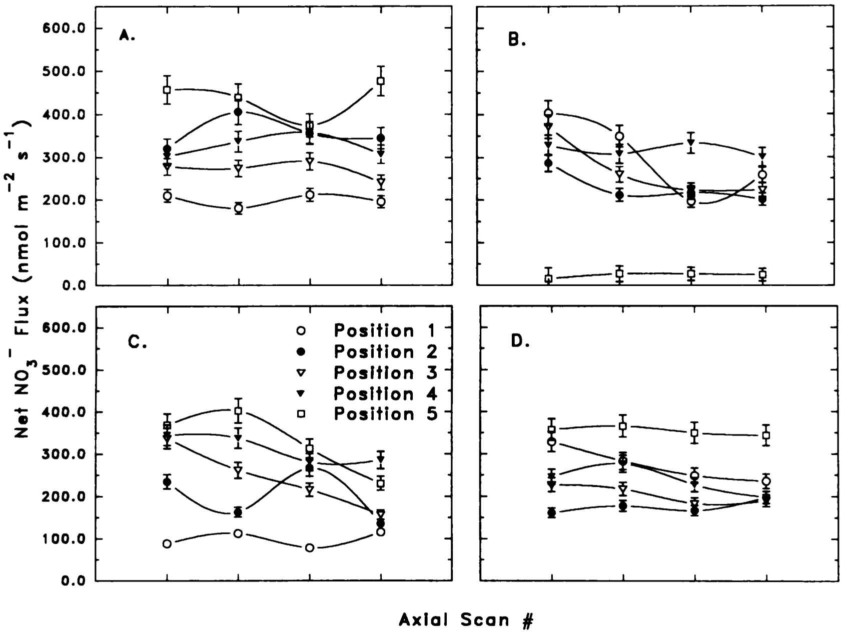

Figure 10. Variations in NO$_3^-$ net flux over time at each position. Axial scans of net fluxes of NO$_3^-$ were made at five positions along the apical 7 cm of intact, 7-d-old barley seedlings. A complete scan was made every 90 min, and four scans were conducted on each root. Each panel (A, B, C, and D) represents a single root from a different plant. Lettered panels correspond to panels in Figure 9. Error bars represent 95% confidence based on system uncertainty calculations. The data points have been interpolated with cubic spline curves.

barley roots in response to gentle physical disturbance; reduced uptake was observed for 2 to 12 h, depending on the nutritional pretreatment of the plants. We have, therefore, made it a practice to insert plants into our experimental chamber at least 12 h before the start of an experiment.

Although the spatial resolution of previous techniques has been generally adequate, it has not been possible to observe changes in the rate of uptake during the course of the experiment. Inasmuch as these techniques all produce a summary of total tracer accumulation along the root axis during the duration of the experiment, little insight is provided concerning variations in uptake with time. In contrast, the MFET provides a very effective method for observing temporal variations in ion uptake along the root axis. The technique is noninvasive and nonperturbing and, therefore, allows repeated measurements at various positions along the root axis during an extended period of time.

Current Work

In experiments using the MFET, net NH_4^+ fluxes measured during the first hour of exposure were generally greater than subsequent measurements made at the same position (Fig. 7). Ammonium transport across the plasmalemma has been observed to cause a sharp depolarization of the membrane potential (14) and might, therefore, be expected to reduce the driving force for NH_4^+ transport. However, the decline in net NH_4^+ uptake evident between the first and second axial scans is not a rapid change but, rather, occurs gradually during the course of the first hour of exposure to NH_4^+ (Fig. 7); any membrane potential changes due to NH_4^+ influx were probably complete before the first cycle of measurements could be made. All of the fluxes measured during the first hour are larger than those during the second hour, except near the root apex. Goyal and Huffaker (9) observed a comparable decline in NH_4^+ uptake in wheat seedlings that were grown without nitrogen; after declining for 1 h, net NH_4^+ uptake then increased to a steady rate that was still lower than the initial NH_4^+ uptake rate. Morgan and Jackson (19) also demonstrated a similar reduction in net NH_4^+ uptake in nitrogen-deprived intact wheat seedlings. Using $^{14}NH_4^+$ and $^{15}NH_4^+$, they were able to show that the reduction in net NH_4^+ uptake was due to an increase in NH_4^+ efflux; NH_4^+ influx also increased, although to a lesser extent. The decline in NH_4^+ uptake continued for approximately 5 h, whereupon net NH_4^+ uptake increased to the initial rate during the course of 24 to 34 h.

All of the NH_4^+ axial scans appear to show a slight decline in net NH_4^+ flux with distance from the root apex (Fig. 7). It seems reasonable to view the root apex as a sink for energy and raw materials necessary for the production of new cellular material. Support for this lies in the fact that root respiration levels are highest near the apex (18), as are inorganic nitrogen assimilatory enzyme activities (21). Ammonium is a more direct source of nitrogen for amino acid and protein synthesis than nitrate; less energy is required for both transport and assimilation. In addition, net fluxes of NO_3^- tend to be low near the root apex but increase slightly toward the basal portions of the root (Fig. 9). Cell elongation is driven by turgor pressure, which, in turn, is effected by a lowering of the solute potential (ψ_s). Nitrate is able to function both as an osmoticum and as a mobile ion (25), functions for which NH_4^+ is unsuitable because of its cytotoxic effects (11). The slight increase in net NO_3^- flux with distance from the root apex may be related to accumulation of NO_3^- in vacuoles or with increased translocation of NO_3^- from the root in association with cations.

What is interesting in Figures 7 through 10, however, are the fluctuations in net uptake during short time intervals and the asynchrony in uptake along the root axis; whereas one position shows a reduction in net flux between successive hours, a neighboring position shows an increase (Figs. 8 and 10). Some positions exhibit an alternation in the direction of the change in net flux between successive hours; the net flux increases, decreases, then increases, or *vice versa*. These observations suggest that regulation of ion uptake may occur on a more localized scale than is commonly thought. It appears that regions along the root axis may vary significantly in whatever metabolic conditions regulate the uptake of inorganic nitrogen. In the case of NO_3^-, uptake regulation has been proposed to be related to vacuolar $[NO_3^-] + [Cl^-]$ (8), root carbohydrate status (6), and/or cytoplasmic amino acid pools (4). Clarkson (7) suggested a joint regulation of NO_3^- uptake, whereby cytoplasmic $[NO_3^-]$ influences NO_3^- efflux and the cytoplasmic amino acid pool influences NO_3^- influx. The regulation of ammonium uptake has received less attention, although it is likely that cytoplasmic amino acid pools and the availability of carbon skeletons will figure prominently in regulatory mechanisms. Apparently, these conditions vary within relatively short distances along the root axis and during observably short time periods.

CONCLUSIONS

The MFET enables determination of net ion uptake with high spatial and temporal resolution and affords a high degree of accuracy if appropriate precautions are taken: an accurate micropositioning device and a high resolution optical system are required to position the microelectrode tip, electrode fabrication techniques must produce electrodes with low drift and virtually constant slope, the experimental apparatus must be electrically shielded to minimize noise and maximize the accuracy of the emf measurements, the contribution of electrical potentials to the microelectrode emf must be assessed, and transpiration rates should be estimated to determine whether Equation 8 or Equation 13 is applicable.

With the MFET we have been able to observe net fluxes of NH_4^+ and NO_3^- along the root axis of intact barley seedlings with a high degree of spatial resolution. It should be noted that the spatial resolution of the MFET is limited by the diffusion of ions in an axial direction and not by the relatively small tip diameter of the microelectrode. We have demonstrated (Figs. 5 and 6) that the spatial resolution depends on the distance from the root surface at which measurements are made. The MFET appears to be one of the only ways to detect changes in net uptake along the root axis during relatively short time periods. Furthermore, aspects of previous techniques that disturb normal root function and, therefore, cloud experimental results have been reduced; measurements were made on intact roots that were grown on a complete nutrient solution and were given sufficient time to recover from handling and perturbations before the start of each experiment.

In 1959, despite the disadvantages of then current techniques, Steward and Sutcliffe (29) suggested that "the point, or points, of maximum [ion] accumulation may be located at different distances along the axis of the root, and this may vary with time. . . .there are strong indications that cyclical or rhythmical phenomena, which reflect the periodicity of growth, may influence the location at any one time of the maximum accumulation along the axis of the root" (p 454). The current work reveals the uptake of NH_4^+ and NO_3^- along the root axis to be a dynamic process, exhibiting significant variations over relatively short distances and periods of time. Individual roots showed different patterns of uptake, although net influxes of NH_4^+ and NO_3^- were always observed along the entire apical 7-cm sections measured. Because of the variations in net fluxes observed between adjacent measurement positions, there appears to be a close regulation of uptake, due perhaps to the metabolic state of localized groups of cells. The MFET is one technique that will be of great use in further describing the dynamics of ion uptake and interactions along the axes of intact roots.

ACKNOWLEDGMENTS

The authors wish to express their gratitude to Barbara Bernstein for scientific illustrations past and present; to Dr. Arnold J. Bloom for helpful comments on the manuscript; to the California Crop Improvement Association, Davis, CA, for Prato barley seed; to Dr. Daniel J. Aneshansley for comments concerning system bandwidth calculations; and to Scott T. Meissner for assistance with statistical analysis.

LITERATURE CITED

1. **Bird RB, Stewart WE, Lightfoot EN** (1960) Transport Phenomena. John Wiley & Sons, Inc., New York, pp 126, 495–555
2. **Bloom AJ, Caldwell RM** (1988) Root excision decreases nutrient absorption and gas fluxes. Plant Physiol **87:** 794–796
3. **Bloom AJ, Sukrapanna SS** (1990) Effects of exposure to ammonium and transplant shock upon the induction of nitrate absorption. Plant Physiol **94:** 85–90
4. **Breteler H, Siegerist M** (1984) Effect of ammonium on nitrate utilization by roots of dwarf bean. Plant Physiol **75:** 1099–1103
5. **Carslaw HS, Jaeger JC** (1959) Conduction of Heat in Solids, Ed 2. Oxford University Press, New York, pp 221, 339
6. **Champigny ML, Talouizte A** (1986) Dependence of nitrate reduction on root soluble carbohydrates in wheat seedlings. *In* H Lambers, JJ Neeteson, I Stulen, eds, Fundamental, Ecological and Agricultural Aspects of Nitrogen Metabolism in Higher Plants, Developments in Plant and Soil Sciences, Vol 19. Martinus Nijhoff Publishers, Boston, MA, pp 279–282
7. **Clarkson DT** (1986) Regulation of the absorption and release of nitrate by plant cells: a review of current ideas and methodology. *In* H Lambers, JJ Neeteson, I Stulen, eds, Fundamental, Ecological and Agricultural Aspects of Nitrogen Metabolism in Higher Plants, Developments in Plant and Soil Sciences, Vol 19. Martinus Nijhoff Publishers, Boston, MA, pp 3–27
8. **Cram WJ** (1973) Internal factors regulating nitrate and chloride influx in plant cells. J Exp Bot **24:** 328–341
9. **Goyal SS, Huffaker RC** (1986) The uptake of NO_3^-, NO_2^-, and NH_4^+ by intact wheat (*Triticum aestivum*) seedlings. I. Induction and kinetics of transport systems. Plant Physiol **82:** 1051–1056
10. **Grasmanis VO, Barley KP** (1969) The uptake of nitrate and ammonium by successive zones of the pea radicle. Aust J Biol Sci **22:** 1313–1320
11. **Haynes RJ** (1986) Uptake and assimilation of mineral nitrogen by plants. *In* RJ Haynes, Mineral Nitrogen in the Plant-Soil System. Academic Press, Inc., New York, pp 303–379
12. **Haynes RJ** (1990) Active ion uptake and maintenance of cation-anion balance: a critical examination of their role in regulating rhizosphere pH. Plant Soil **126:** 247–264
13. **Henriksen GH, Bloom AJ, Spanswick RM** (1990) Measurement of net fluxes of ammonium and nitrate at the surface of barley roots using ion-selective microelectrodes. Plant Physiol **93:** 271–280
14. **Higinbotham N, Etherton B, Foster RJ** (1964) Effect of external K, NH_4, Na, Ca, Mg, and H ions on the cell transmembrane electropotential of *Avena* coleoptile. Plant Physiol **39:** 196–203
15. **Johnson CM, Stout PR, Broyer TC, Carlton AB** (1957) Comparative chlorine requirements of different plant species. Plant Soil **8:** 337–353
16. **Kline SJ, McClintock FA** (1953) Describing uncertainties in single sample experiments. Mech Eng **75:** 3–8
17. **Koster AL** (1963) Changes in metabolism of isolated root systems of soy bean. Nature **198:** 709–710
18. **Machlis L** (1944) The respiratory gradient in barley roots. Am J Bot **31:** 281–282
19. **Morgan MA, Jackson WA** (1988) Inward and outward movement of ammonium in root systems: transient responses during recovery from nitrogen deprivation in presence of ammonium. J Exp Bot **39:** 179–191
20. **Newman IA, Kochian LV, Grusak MA, Lucas WJ** (1987) Fluxes of H^+ and K^+ in corn roots. Characterization and stoichiometries using ion-selective microelectrodes. Plant Physiol **84:** 1177–1184
21. **Oaks A, Stulen I, Jones K, Winspear MJ, Misra S, Boesel IL** (1980) Enzymes of nitrogen assimilation in maize roots. Planta **148:** 477–484
22. **Press WH, Flannery BP, Teukolsky SA, Vetterling WT** (1989) Numerical Recipes in Pascal. The Art of Scientific Computing. Cambridge University Press, New York, pp 197–201
23. **Raven JA, Smith FA** (1976) Nitrogen assimilation and transport in vascular land plants in relation to intracellular pH regulation. New Phytol **76:** 415–431
24. **Ryan PR, Newman IA, Shields B** (1990) Ion fluxes in corn roots measured by microelectrodes with ion-specific liquid membranes. J Membr Sci **53:** 59–69
25. **Salsac L, Chaillou S, Morot-Gaudry J-F, Lesaint C, Jolivet E** (1987) Nitrate and ammonium nutrition in plants. Plant Physiol Biochem **25:** 805–812
26. **Sanderson J** (1983) Water uptake by different regions of the barley root. Pathways of radial flow in relation to development of the endodermis. J Exp Bot **34:** 240- 253
27. **Schulze E-D, Bloom AJ** (1984) Relationship between mineral nitrogen influx and transpiration in radish and tomato. Plant Physiol **76:** 827–828
28. **Steward FC** (1948) Metabolism and salt uptake by plants—some problems and precepts for the application of radioactive isotopes. *In* Brookhaven Conference Report BNL-C-4: Biological Applications of Nuclear Physics. Brookhaven National Laboratory, Upton, NY, pp 94–103
29. **Steward FC, Sutcliffe JF** (1959) The root as an absorbing organ for salts. *In* FC Steward, ed, Plant Physiology, A Treatise, Vol 2. Academic Press, New York, pp 453–457
30. **Weisenseel MH, Dorn A, Jaffe LF** (1979) Natural H^+ currents traverse growing roots and root hairs of barley (*Hordeum vulgare* L.). Plant Physiol **64:** 512–518
31. **Wiebe HH, Kramer PJ** (1954) Translocation of radioactive isotopes from various regions of roots of barley seedlings. Plant Physiol **29:** 342–348